Experimental Validations of Time-Domain Voltage/Current Control: Electrical Correction of Faulty Transmission-Line Networks

Ali Al Ibrahim, Cédric Chauvière, and Pierre Bonnet

***Abstract*— This article is dedicated to experimentally validating the linear combination of the configuration field (LCCF) method in transmission-line (TL) networks. The LCCF is first modified to comply with some physical limitations encountered during experimentation and then tested to identify the temporal profile of voltage/current sources that would lead to specified voltage/current signals over a definite time interval at a few points of a TL network. In another experimental validation, when faults appear in some lines of these networks, the LCCF is also tested to bring an electrical correction (EC) that compensates for the effect of the potential faults regardless of the number, nature, and position. For this latter, soft and hard faults are considered. The LCCF method paves the way for the development of new instrumentation in generating and conditioning temporal signals.**

***Index Terms*— Complex wire networks, electrical correction (EC), fault, source identification, time-domain analysis.**

I. Introduction

IN THE last decades, source identification problems to generate a desired electromagnetic field in an area of interest have considerably received the attention of researchers and engineers [1], [2], [3]. Accordingly, different applications and research studies, especially those related to electromagnetic compatibility (EMC), have emerged. In the frequency-domain analysis, many methods based on the equivalence principle and genetic algorithms, for instance, were developed to substitute or replace real complex sources by a few equivalent radiating electric or magnetic dipoles [4], [5], [6]. Similarly, the electromagnetic source identification to cancel, reduce, or replace any unintentional emissions with the desired ones or complex radiations with their equivalents is also a challenging inverse-source problem (ISP) [7].

ISPs are defined as the processes of estimating data that may not directly be acquired by measurements. With a set of physical quantities' measurements and observations, ISPs compute the casual input parameters of the physical system that produced these quantities. As a matter of fact, ISPs showed signs of instability, ill-posedness, and ill-conditionality. For these reasons, the electromagnetic sources were alternatively identified by solving optimization problems (e.g., least squares [8] and the conjugate gradient [9] methods) or by solving partial differential equations (e.g., Hilbert uniqueness method [10]).

Although all the previously mentioned methods have shown to be efficient at identifying sources in the frequency domain, they are still very general and may reveal serious complications during implementations. Moreover, they have shown to be less reliable when tackling problems in the time domain [11]. In fact, developing time-domain methods becomes essential due to the appearance of large numbers of practical time-dependent problems. For this purpose, researchers devoted much effort to developing other efficient time-domain techniques, such as time reversal (TR). In the early 1990s, the TR approach was first introduced to refocus acoustic waves in the time domain [12]. Later, the TR was invested in EMC problems (e.g., source identification, fault detection, and location) to refocus electromagnetic waves by reversing in time the response signals of a system [13], [14], [15], [16]. Although the TR shows to be efficient at identifying temporal sources at a unique point in the medium and the focusing instant only, its performance, unfortunately, weakens when imposing complex conditions on the duration or the profile of the refocused electromagnetic field [17]. Moreover, TR applicability becomes unsteady when applied in lossy or constrained environments due to the poor refocusing quality of the back-propagated signals [18], [19]. Besides identifying sources, the TR was also successfully applied to detect and locate faults in power networks [20] and transmission-line (TL) networks [21], [22], [23].

Sooner or later, a cable in a network will inevitably show signs of weakness attributed to either external factors (e.g., mechanical stress, humidity, etc.) or internal reasons (overheating, corrosion, insulation damage, etc.). These deteriorations result in the modification of the EMC characteristics of the overall system, affecting the immunity and emissivity of its wires. These faults may be categorized into hard faults (open and short circuits) and soft faults (chafing, cracks, frays, etc.). Among the most well-suited methods to detect and locate electrical faults in TL networks are the reflectometry-based techniques [24]. However, they present some limitations

Manuscript received 13 June 2023; revised 14 July 2023; accepted 22 July 2023. Date of publication 8 September 2023; date of current version 12 September 2023. This work was supported in part by the Contrat Plan Etat Région (CPER) Mobilités, Matériaux et Systèmes du Futur (MMASYF) of the Auvergne-Rhône Alpes Region and the European Commission (Fonds Européen de Développement Régional (FEDER) Auvergne Funds). The Associate Editor coordinating the review process was Dr. Tarikul Islam. *(Corresponding author: Ali Al Ibrahim.)*

Ali Al Ibrahim and Pierre Bonnet are with the Université Clermont Auvergne, Clermont Auvergne INP, CNRS, Institut Pascal, F-63000 Clermont-Ferrand, France (e-mail: ali.al_ibrahim@uca.fr; pierre.bonnet@uca.fr).

Cédric Chauvière is with the Université Clermont Auvergne, Clermont Auvergne INP, CNRS, Laboratoire de Mathématiques, F-63000 Clermont-Ferrand, France (e-mail: cedric.chauviere@uca.fr).

Digital Object Identifier 10.1109/TIM.2023.3304680

when it comes to tackling soft faults, complex, or lossy networks [25]. The TR and reflectometry-based techniques may detect and locate faults that could not be repaired due to external factors, such as hard-to-access zones (e.g., network with faults in its wires located in a radioactive zone, or a faulty network of a satellite in outer space). Furthermore, some faults, such as those in underground or subsea cables, may not be immediately accessible for maintenance operations. In this case, once faults are detected, the electrical systems are often shut down to avoid exposure to potential risks or damages. This precautionary measure can ultimately result in time losses and financial revenue reductions.

For all these reasons, it becomes essential to develop new paradigms, such as electrical correction (EC), dedicated to compensating for the effects of the faults in wiring networks and handling them as a part of the network's topology without any need to access their location or acquire information about them. The EC is the process of remotely compensating for the effects of potential faults without any physical intervention. This may be done by adding new inputs to the initial signal in a faulty network to deliver the same output signals as the healthy network.

In 2012, a novel linear combination of the configuration field (LCCF) method was introduced [26] and then applied to TL networks [27]. The main purpose of the primary LCCF is to compute a source that when emitted, controls the voltage, current, or electromagnetic field at one space point over a definite time interval. In other words, after the computed source propagates, it generates a desired voltage/current or field at a space point in reverberating environments [26] or wiring networks [27]. Later, the LCCF was generalized to control electromagnetic fields at several space points in reverberating cavities [28] and voltage/current in TL networks [29]. For this latter, the LCCF was also used to bring an EC to the terminations of faulty TL networks [29]. The work achieved in [29] was purely numerical, whether for voltage/current control or the EC application.

Interestingly, the LCCF method has been successfully experienced in a reverberating cavity [28]; however, it was never tested in TL networks. That is why, in this contribution, we go a step further and conduct the first experimental tests in TL networks to demonstrate the LCCF method's validity for both generating a desired voltage/current and bringing an EC at the terminations of the networks. The LCCF in this article deals with analog time-varying voltage or current signals in TL networks, where our focus lies not on signals in the conventional sense of information transmission but rather on current or voltage signals. The objective is not to perform post-hoc correction of transmitted information but rather to directly manipulate the electrical signal itself to ensure compliance with potential EMC constraints by sustaining the waveform characteristics (such as amplitude, waveform shape, frequency spectrum, etc.). The LCCF technique, similar to TR, relies on an adequate conditioning signal [30] that acts as a source for improved signal transmission. The main novelties and improvements presented in this article include the experimental validation of the LCCF for addressing original problems in TL networks and providing a practical solution for injecting an ideal Dirac pulse. It should be declared that this article reuses some content from thesis [31] with permission.

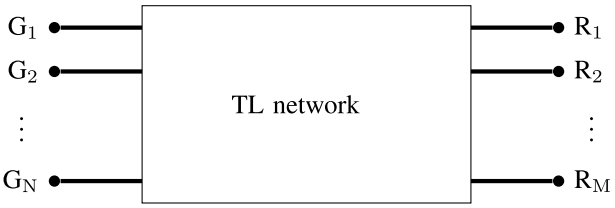

Fig. 1. TL network with N generators $G_1, \ldots, G_N$ (inputs) and M receivers $R_1, \ldots, R_M$ (outputs).

The article is structured as follows: In Section II, the LCCF theory is presented and then modified in Section III to comply with physical limitations one encounters during experiments. After describing the experimental setup in Section IV, the LCCF method is applied in Sections V and VI to, respectively, control voltage/current in TL networks and bring an EC when faults appear in the network, independent of their number, nature, and position.

II. Generalized LCCF Method

A. Settings

To better understand the generalized LCCF method in wiring networks, its schematic setup is represented in Fig. 1. We consider the time-discrete propagation of voltage or current in a linear system with arbitrary transmission lines (coaxial, multiwired, bundled, shielded, or unshielded cables). Let us denote by Δt the time step of discretization and t_n the last instant of time to be specified, where $t_n = n\Delta t > 0$ ($n \in \mathbb{N}^*$). For all $t \in [0, t_n]$, the source generators $\mathrm{G}_1, \ldots, \mathrm{G}_N$ emit $N \in \mathbb{N}^*$ nonnull input signals $\mathbf{x}_1, \ldots, \mathbf{x}_N$, respectively. For all $j \in \{1, \ldots, N\}$, $\mathbf{x}_{j/_{[0,t_n]}} = [x_j(0), \ldots, x_j(n)] \in \mathbb{R}^{n+1}$. The signals $\mathbf{x}_1, \ldots, \mathbf{x}_N$ propagate, interfere, and may be distorted due to junctions and mismatched impedance of the network. A set of $M \in \mathbb{N}^*$ receivers $\mathrm{R}_1, \ldots, \mathrm{R}_M$ are placed at M distinct points, where each records the signal it detects over $[0, t_n]$. These output signals are denoted by $\mathbf{y}_1, \ldots, \mathbf{y}_M \in \mathbb{R}^{n+1}$ detected by $\mathrm{R}_1, \ldots, \mathrm{R}_M$, respectively. For all $i \in \{1, \ldots, M\}$, $\mathbf{y}_{i/_{[0,t_n]}} = [y_i(0), \ldots, y_i(n)] \in \mathbb{R}^{n+1}$.

B. Description

The ultimate objective of the generalized LCCF method is to identify $\mathbf{x}_1, \ldots, \mathbf{x}_N$ that may simultaneously control $\mathbf{y}_1, \ldots, \mathbf{y}_M$ over a definite interval of time. This time interval is called the "target time" and denoted by $[t_q, t_f] = [q\Delta t, f\Delta t] \subseteq [0, t_n]$, where $(q, f) \in \mathbb{N}^* \times \mathbb{N}^*$. To control $\mathbf{y}_1, \ldots, \mathbf{y}_M$ over $[t_q, t_f]$ means to impose predefined target fields $\mathbf{F}_1, \ldots, \mathbf{F}_M$ at the M-receiver points over $[t_q, t_f]$. Then, the LCCF method is based on solving the following linear system:

$$\mathbf{A}\mathbf{x} = \mathbf{F} \tag{1}$$

where

1) $\mathbf{x} = (\mathbf{x}_1, \ldots, \mathbf{x}_N)^T$ with $\mathbf{x}_j \in \mathbb{R}^{f+1}$ the vector to be computed containing the discrete data of the source emitted by G_j. Note that $\mathbf{x}_{j/_{[t_{f+1}, t_n]}} = \mathbf{0}$ as these amplitudes reach

the receiver points after $[t_q, t_f]$ and therefore have no impact on $\mathbf{y}_{i/_{[t_q,t_f]}}$.

2) $\mathbf{F} = (\mathbf{F}_1, \ldots, \mathbf{F}_M)^T$ with $\mathbf{F}_i \in \mathbb{R}^{f-q+1}$ being the vector representing the discrete data of the target voltage/current to be imposed at R_i-point over $[t_q, t_f]$ after the emission of $\mathbf{x}_1, \ldots, \mathbf{x}_N$

3)
$$\mathbf{A} = \begin{pmatrix} \mathbf{A}_{11} & \cdots & \mathbf{A}_{1N} \\ \vdots & \ddots & \vdots \\ \mathbf{A}_{M1} & \cdots & \mathbf{A}_{MN} \end{pmatrix}$$
is a block matrix with $\mathbf{A}_{ij} \in \mathbb{M}_{(f-q+1)\times(f+1)}$ being the rectangular real matrix that characterizes the medium between the two fixed G_j-point and R_i-point. A comprehensive explanation of how to construct $\mathbf{A}_{ij}$ can be found in [26].

The reader may also refer to [29] for a detailed description of the generalized LCCF method. The LCCF system (1) is not square and may be solved for $\mathbf{x}$ in the least-square sense by premultiplying both sides by $\mathbf{A}^T$. The matrix $\mathbf{A}^T\mathbf{A}$ is ill-conditioned, then we use Tikhonov regularization [34] to stabilize the LCCF system

$$(\mathbf{A}^T\mathbf{A} + \epsilon\mathbf{I})\mathbf{x} = \mathbf{A}^T\mathbf{F}. \tag{2}$$

The Tikhonov parameter $\epsilon > 0$ is heuristically chosen to be small enough so as not to distort the solution.

III. Experimental LCCF Method

Due to some physical limitations during experimentation, the generalized LCCF method in its version described above may not be applicable to conduct tests. These tests may not be carried out unless the LCCF is modified to comply with such limitations. First of all, the recorded impulse responses used to construct the matrix $\mathbf{A}$ may be theoretically and numerically convenient, but not experimentally. This is due to the impossible emission of the Dirac signal $\boldsymbol{\delta}$ during experimental tests. As an alternative solution, $\mathbf{A}$ may be built using the responses of any incident signal denoted by $\boldsymbol{\alpha} = [\alpha(0), \ldots, \alpha(n)] \neq \boldsymbol{\delta}$ that is experimentally feasible.

Previously, in [28], the experimental description of the LCCF method was given for one generator point and two receiver points. In this section, the experimental representation of the LCCF is generalized for N generator points and M receiver points. Let $\tilde{A}$ be the matrix constructed in exactly the same way as $\mathbf{A}$, but, this time, based on the responses of $\boldsymbol{\alpha}$ and not the impulse responses. Considering the new notation, the LCCF system may be written after Tikhonov regularization as follows:

$$(\tilde{A}^T\tilde{A} + \epsilon\mathbf{I})\tilde{x} = \tilde{A}^T\mathbf{F}. \tag{3}$$

Solving system (3) will compute a set of sources $\tilde{x} = (\tilde{x}_1, \ldots, \tilde{x}_N)^T \neq \mathbf{x}$. In reality, injecting the sources $\tilde{x}_j$ simultaneously, each by its generator, does not produce the target signals $\mathbf{F}_1, \ldots, \mathbf{F}_M$ at the receiver points since $\tilde{A}$ is not the characterization matrix of the LCCF system. That is why it is necessary to compute $\mathbf{x}_j$ from $\tilde{x}_j$ using basic concepts of linear algebra. As a matter of fact, each source $\tilde{x}_j$ is the expression of its corresponding solution $\mathbf{x}_j$, computed on another basis. Let $\boldsymbol{\alpha}_{k\in\{1,\ldots,f+1\}}$ be a signal, such that $\boldsymbol{\alpha}_k = [\mathbf{0}_{k-1}, \alpha(0), \ldots, \alpha(f-k+1)]$. Denote by $\mathscr{C} = \{\boldsymbol{\delta}_1, \ldots, \boldsymbol{\delta}_{f+1}\}$ the canonical basis of the vector space $\mathbb{R}^{f+1}$. Assuming that $\mathscr{B} = \{\boldsymbol{\alpha}_1, \ldots, \boldsymbol{\alpha}_{f+1}\}$ forms also a basis of $\mathbb{R}^{f+1}$, then there exists an invertible matrix $\mathbf{P}$ called the transition matrix from $\mathscr{C}$ to $\mathscr{B}$, such that $\boldsymbol{\alpha}_k = \mathbf{P}\boldsymbol{\delta}_k$, where

$$\mathbf{P} = \begin{bmatrix} \boldsymbol{\alpha}_1 \cdots \boldsymbol{\alpha}_{f+1} \end{bmatrix} = \begin{pmatrix} \alpha(0) & 0 & \cdots & 0 \\ \vdots & \ddots & \ddots & \vdots \\ \vdots & & \ddots & 0 \\ \alpha(f) & \cdots & \cdots & \alpha(0) \end{pmatrix}. \tag{4}$$

Each vector $\mathbf{x}_j$ is a linear combination of $\tilde{x}_j(0), \ldots, \tilde{x}_j(f)$ in $(\mathbb{R}^{f+1}, \mathscr{B})$ and may be written in $(\mathbb{R}^{f+1}, \mathscr{C})$ as follows:

$$\mathbf{x}_j = \sum_{k=1}^{f+1} \tilde{x}_j(k-1)\boldsymbol{\alpha}_k = \mathbf{P}\sum_{k=1}^{f+1} \tilde{x}_j(k-1)\boldsymbol{\delta}_k = \mathbf{P}\tilde{x}_j. \tag{5}$$

Hence, $\mathbf{x} = \boldsymbol{\mathscr{P}}\tilde{x}$, where $\boldsymbol{\mathscr{P}} \in \mathbb{M}_{N\times N}$ is a block diagonal matrix, such that $\boldsymbol{\mathscr{P}}_{jj} = \mathbf{P}$. It is noteworthy that many nonnull signals can be used to experimentally construct $\mathbf{A}$. For the sake of simplicity, only one source point is considered in our experiments, that is, $N = 1$; however, the experiments remain valid for any number of source points, that is, $N > 1$.

In general, the LCCF may always compute a source $\mathbf{x}$ (if exists) that is mathematically correct; however, this source may not physically be satisfying for experimental tests due to some physical drawbacks, such as the high amplitudes or high frequencies of $\mathbf{x}$. In the following, we will not deal with such limitations although the reader may still refer to [29], [35], and [33] for proposed solutions.

IV. Experimental Setup

To experimentally test the LCCF method, linear wiring networks are considered. Indeed, any network of any arbitrary topology can be used for the two experimental validations illustrated in this article: control voltage/current and EC in wiring networks. We consider voltage signals in our tests; however, current signals can also be considered in a similar way.

A Tektronix AWG70002A arbitrary waveform generator[1] (AWG), represented in Fig. 2(a), is connected to the network at one of its ports to generate any arbitrary shape signal up to 25 GSa/s in an amplitude range [−250 and +250 mV]. The M receiver points are the network's terminations connected to M channels of the oscilloscope $\mathrm{CH}_1, \mathrm{CH}_2, \ldots, \mathrm{CH}_M$. As an example, the number of the receiver points is taken to be equal to two ($M = 2$). The network's terminations connected to the AWG, CH_1, and CH_2 are chosen randomly; undoubtedly, any other connection between any termination and any electronic component is still possible. The oscilloscope coupling at the receiver points is chosen to be 1dc MΩ. In fact, any coupling may certainly be selected as it is

[1]The AWG was supported by the CPER MMASYF of the Auvergne-Rhône Alpes Region and the European Commission (FEDER Auvergne Fund).

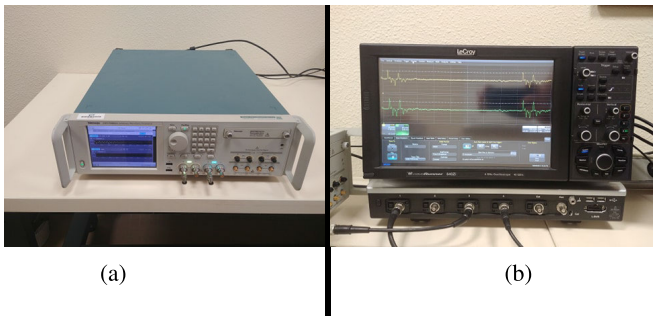

(a) (b)

Fig. 2. Equipment used in experiments. (a) Arbitrary waveform generator. (b) Oscilloscope.

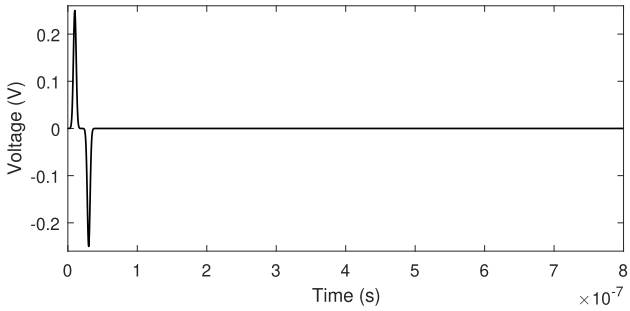

Fig. 3. Incident signal $\boldsymbol{\alpha}$ used instead of the Dirac signal.

included in the network's characteristics of which the LCCF is independent. Similarly, all other characteristics of the system (e.g., cable losses, mismatched junctions, and terminations) are also involved in the matrix $\mathbf{A}$. The oscilloscope used is a LeCroy WaveRunner 640Zi [see Fig. 2(b)] with a frequency range from 400 MHz to 4 GHz. It is responsible for displaying the variation of the voltage signals as a function of time. The signal emissions and recordings are synchronized using a trigger signal.

As reported earlier, it is not possible to record the impulse response experimentally due to the impractical excitation of the Dirac signal. However, we may rely on the response of any other nonnull and nonconstant incident pulse $\boldsymbol{\alpha}$, as long as its amplitudes respect the amplitude range of the generator, and its frequencies fall within the bandwidth of the oscilloscope. For instance, the pulse $\boldsymbol{\alpha}$ is chosen to be the signal displayed in Fig. 3. Yet, any other signal can still be chosen as long as it complies with the limitations imposed by the available equipment. The responses of $\boldsymbol{\alpha}$ should be recorded again whenever the network's configuration undergoes any modification.

V. Control Voltage/Current in Wiring Networks

In this section, we describe the network under consideration, then present a direct experiment of the LCCF method. That is to say, we identify the temporal profile of a voltage source $\mathbf{x}$ that, when injected, produces a desired target signal at the receiver points over the target time $[t_q, t_f]$. The signals in this section are controlled over a short target time for illustration purposes, though controlling voltage signals over a given time interval with control loss outside makes little sense in practice. However, as shown in Section VI, the voltage signals can be controlled over the entire time interval.

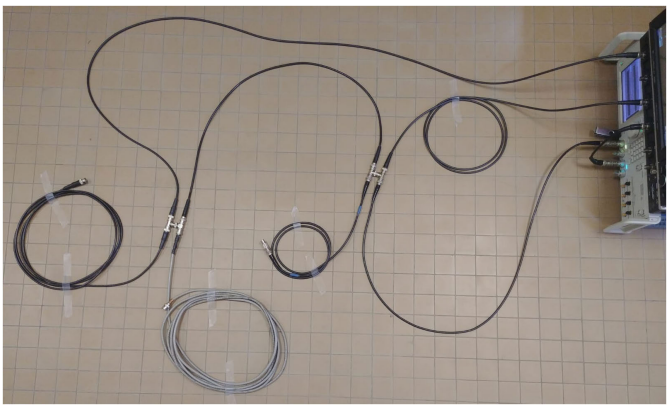

(a)

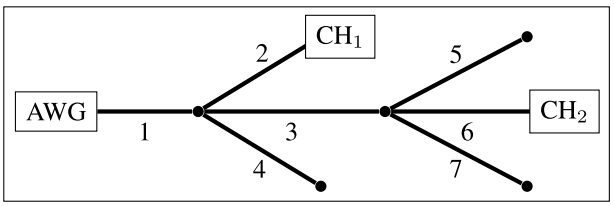

(b)

Fig. 4. Complex network configuration used to control voltage signals. (a) Network configuration. (b) Schematic of the network.

TABLE I
Characteristics of the Network of Fig. 4

Line Nb.	Length (in m)	Z_C (in Ω)	Z_L (in Ω)
1	1.2	50	-
2	2	50	50
3	1	50	-
4	1.2	50	∞
5	5.5	50	∞
6	2	50	50
7	3	50	∞

A. Network Configuration

Consider the network, denoted by Ω, composed of two nodes and seven standard 50 Ω coaxial cables (see Fig. 4). The cables' length, characteristic impedance Z_C, and load impedance Z_L are represented in Table I. To demonstrate that the LCCF method efficiently operates in complex systems, the complex behavior of the network is guaranteed. To do so, three terminations are chosen to be open circuits ($Z_L = \infty$), while Z_L is matched (=50 Ω) at the points connected to the electronic components (AWG, CH_1, and CH_2).

B. LCCF Experiment

The LCCF method is applied to simultaneously impose the Gaussian target voltage signal $\mathbf{G}$ represented in Fig. 5 at the two terminations, CH_1 and CH_2, over the target time $[t_q, t_f]$ lying between 0.4 and 0.48 μs. The responses recorded at CH_1 and CH_2, after injecting $\boldsymbol{\alpha}$ in Ω by the AWG, are, respectively, displayed in Figs. 5(a) and (b), respectively. These two responses are used to construct the LCCF transfer matrices $\mathbf{A}_{ij}$ between the AWG and the receiver points.

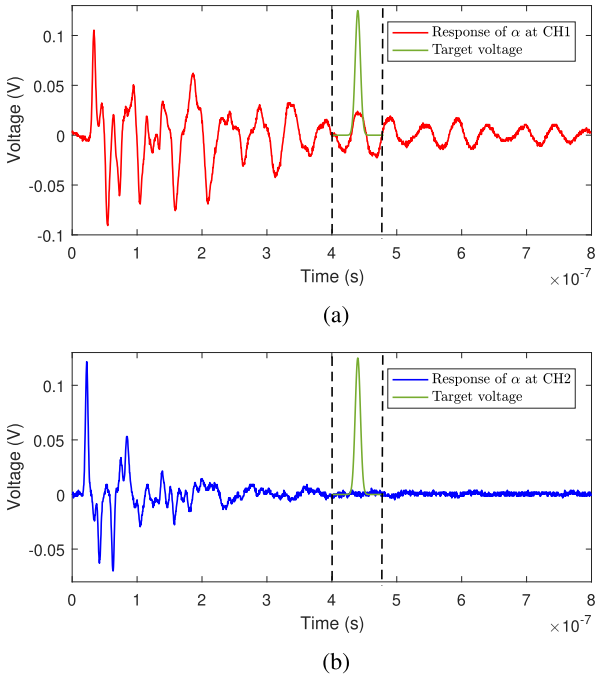

Fig. 5. Responses of the signal $\boldsymbol{\alpha}$ used to characterize the network at CH_1 and CH_2. The Gaussian signal is the target signal to be imposed at the target time $[t_q, t_f] = [0.4\ \mu s, 0.48\ \mu s]$ lying between the two dashed lines. (a) Response of $\boldsymbol{\alpha}$ at CH_1. (b) Response of $\boldsymbol{\alpha}$ at CH_2.

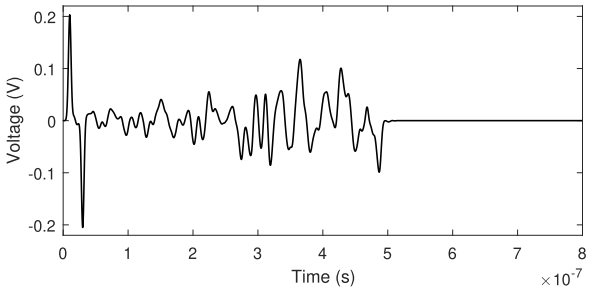

Fig. 6. Source $\mathbf{x}$ computed by the LCCF method.

Here, we are seeking a signal to be injected with or after $\boldsymbol{\alpha}$ to produce $\mathbf{G}$ over $[t_q, t_f]$. The total signal is the source denoted by $\mathbf{x}$ to be computed via the LCCF method. Then, the LCCF system is solved and switched to the canonical basis to compute $\mathbf{x}$ represented in Fig. 6. As expected, the beginning of $\mathbf{x}$ is similar to $\boldsymbol{\alpha}$ due to the effect of this latter. After the injection of $\mathbf{x}$ by the AWG, it propagates through the network, reflects, and re-reflects due to the complex configuration of Ω. At CH_1 and CH_2, the oscilloscope records the signals $\mathbf{y}_1$ and $\mathbf{y}_2$ represented in Figs. 7(a) and (b), respectively. As expected, $\mathbf{y}_1$ and $\mathbf{y}_2$ are almost the Gaussian signal $\mathbf{G}$ over $[t_q, t_f]$. We note that the signals $\mathbf{y}_1$ and $\mathbf{y}_2$ are not controlled before and after the target time; however, they remain in the same order of magnitude as $\mathbf{G}$.

VI. EC in Wiring Networks

The EC, defined as the process to compensate for the effect of faults, may be an alternative solution when detecting faults that are costly or difficult to locate in a TL network. As mentioned in [29], [32], and [33], the EC is not a way

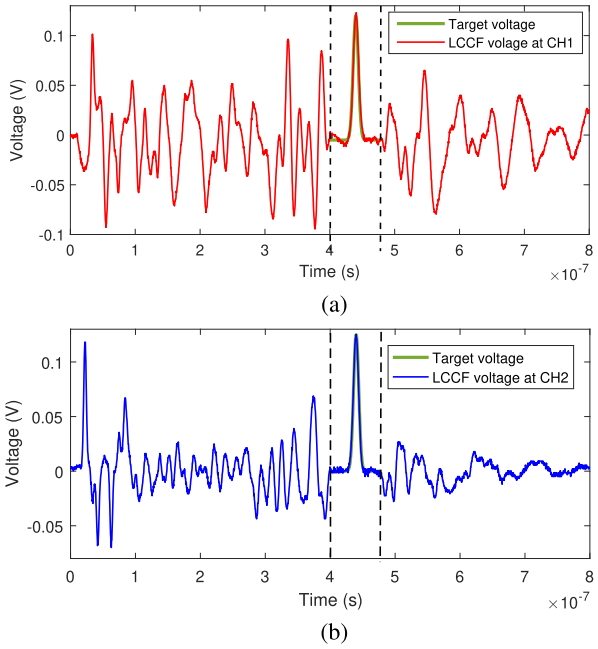

Fig. 7. Signals $\mathbf{y}_1$ and $\mathbf{y}_2$ recorded by the oscilloscope after injecting the source $\mathbf{x}$. The target time $[t_q, t_f]$ is the interval lying between the two dashed lines. (a) Voltage signal $\mathbf{y}_1$ recorded at CH_1 after injecting $\mathbf{x}$. (b) Voltage signal $\mathbf{y}_2$ recorded at CH_2 after injecting $\mathbf{x}$.

to identify the faulty lines or the faults themselves (nature, severity, reflection coefficient, etc.), but to look for a different source transmitted by the generator to eliminate the disturbances (reflections and re-reflections) caused by such faults. The EC concept is summarized in Fig. 8: The input signal injected into the healthy network results in a healthy output, while the injection of the same input signal into a faulty network yields a faulty output signal. Considering these two outputs in conjunction with the input signal, the LCCF signal can be computed. This latter can be combined with the input signal, enabling the recovery of the healthy signal even in the presence of a fault.

In the following, we deal with the same previous setup (see Section IV). The EC process is tested in three separate experiments when the considered network Ω presents faults of various types and locations. The considered simulated fault(s) for each experiment are described as follows.

1) For the first experiment, a soft fault is introduced by mismatching the load impedance at one cable termination of Ω from 50 to 82.5 Ω.
2) For the second experiment, a hard fault is introduced by disconnecting one cable end by removing the 50-Ω resistor (open circuit). Although this test only considers open circuits, short circuits can also be considered.
3) For the third experiment, multiple faults are introduced (a mix of soft and hard faults). More precisely, two faults are modeled in Ω exactly as described in the first and second experiments.

For the sake of notation simplicity, let $\Omega = \Omega_H$ and Ω_F be the healthy and the faulty networks, respectively. The network Ω_F has the same topology and characteristics as Ω_H but with the presence of one or more faults inherent in its cables. The EC

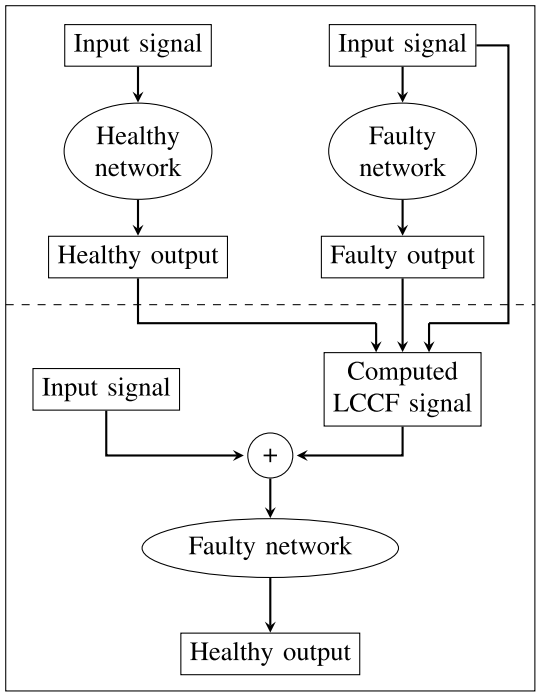

Fig. 8. EC concept.

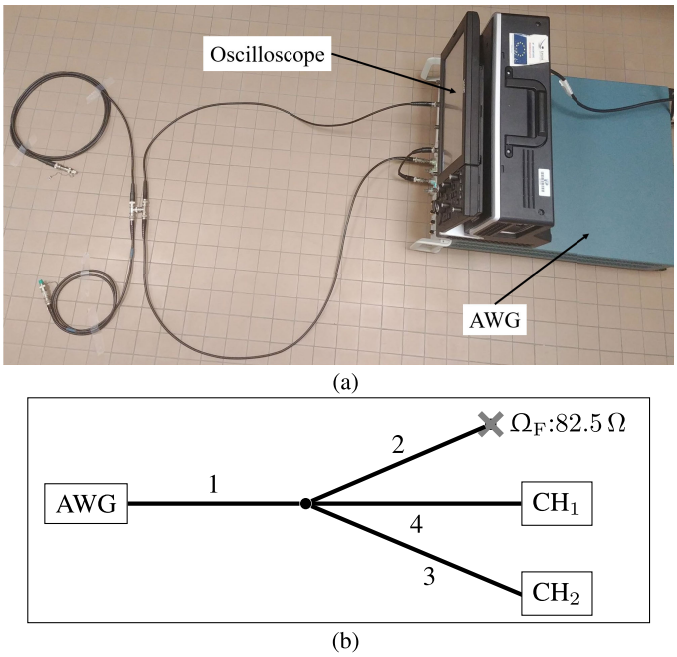

Fig. 9. Network configuration used for the EC process of the single soft fault. (a) Network configuration. (b) Schematic of the network.

may be applied over any target time $[t_q, t_f] \subseteq [0, t_n]$. Herein, we illustrate the EC process over the entire time interval $[0, t_n]$, where $t_n = 0.6$ μs, for instance. In the rest of this article, two different configurations of Ω_H will be considered, each is different from the configuration used in Section V. The purpose is to show that the LCCF method is still applicable to any network cartography and characteristics. For each experiment, we introduce the network configuration used in one subsection and define the way of simulating the fault(s) in another subsection. The faults are actually simulated by locally modifying the resistive loads at the terminations of the cables. Such implementation models faults without deforming the cables, even though the faults may still be located at any position on the network. Finally, we show the results of the EC experimentation obtained via the LCCF method.

A. Soft Fault

Soft faults will evolve sooner or later into hard ones due to many factors, such as aging, humidity, and so on. Consequently, once they are detected, the system is shut down for troubleshooting (identification, location, reparation, etc.), resulting in revenue and time losses. The situation even worsens if the fault is found to be in hard-to-access areas, where reparations are not possible. Then, it becomes crucial to cancel the effect of the soft faults by the EC process to increase the system's lifespan or to maintain its optimal operation until the troubleshooting operation is completed. The EC process is not intended to measure or quantify the soft fault signature evolution over time.

1) Network Configuration: Consider the network Ω_H composed of one node and four standard 50-Ω coaxial cables [see Figs 9(a) and (b)]. The cables' length, Z_C, and Z_L are shown in Table II.

TABLE II
CHARACTERISTICS OF THE NETWORK OF FIG. 9

Line Nb.	Length (in m)	Z_C (in Ω)	Z_L (in Ω)
1	1.2	50	-
2	3	50	50
3	1	50	50
4	1.2	50	50

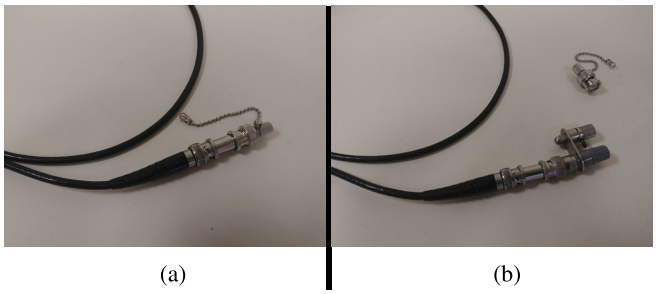

Fig. 10. Replacing the 50-Ω resistor by an 82.5-Ω resistor at the termination of the cable. (a) Healthy termination. (b) Faulty termination.

2) Electrical Correction: To model Ω_F, a soft fault is simulated by replacing the 50-Ω resistor at the end of line 2 [see the gray X-mark in Fig. 9(b)] by an 82.5-Ω resistor, as shown in Fig. 10. After injecting $\boldsymbol{\alpha}$ (Fig. 3) in Ω_H and Ω_F separately, a slight distortion of the outputs at CH_1 and CH_2 is recorded due to the effect of the fault, as displayed in Fig. 11. These outputs are used to construct the LCCF transfer matrices and consequently, the LCCF system that, when solved and switched to the canonical basis, computes the source $\mathbf{x}$ displayed in Fig. 12. The signal $\mathbf{x}$, after being injected in Ω_F, corrects the outputs at CH_1 and CH_2, as seen in Fig. 11.

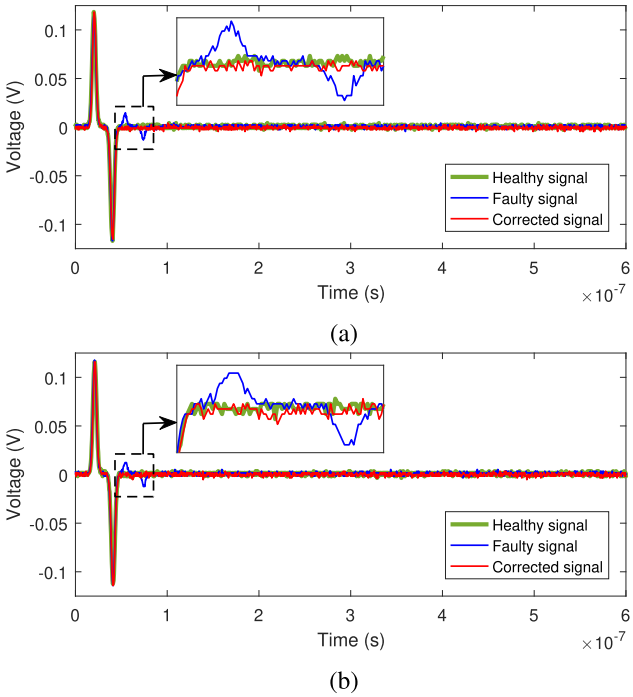

Fig. 11. Experimental EC of the faulty network presenting a single soft fault. (a) Healthy, faulty, and corrected voltage signals at CH_1. (b) Healthy, faulty, and corrected voltage signals at CH_2.

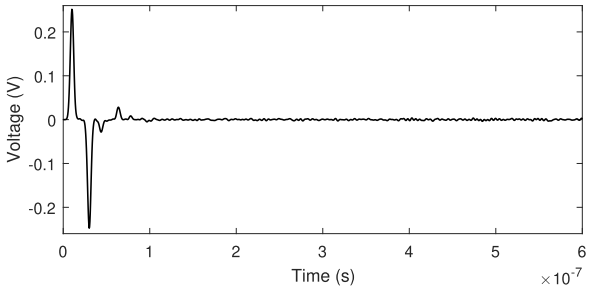

Fig. 12. Source $\mathbf{x}$ computed to correct the outputs in the presence of a single soft fault.

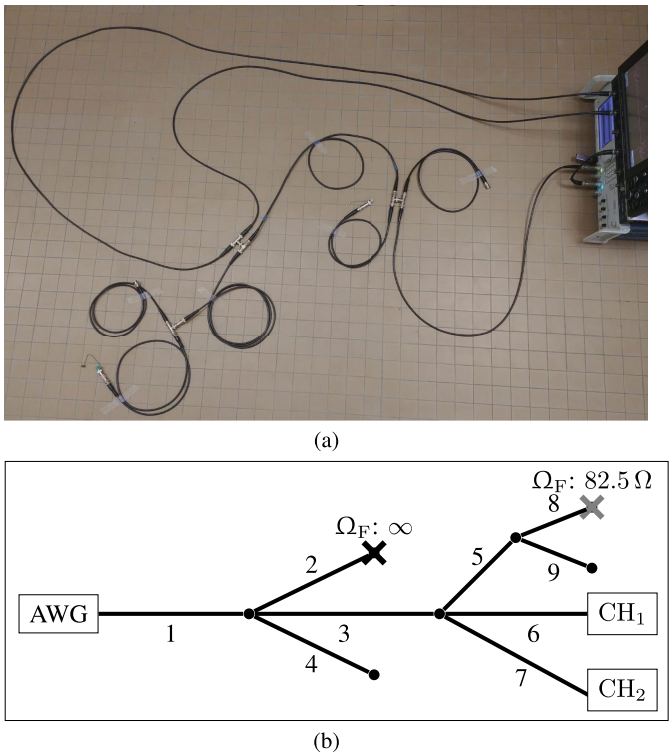

Fig. 13. Network configuration used for the EC process of the single hard fault and multiple faults. (a) Network configuration. (b) Schematic of the network.

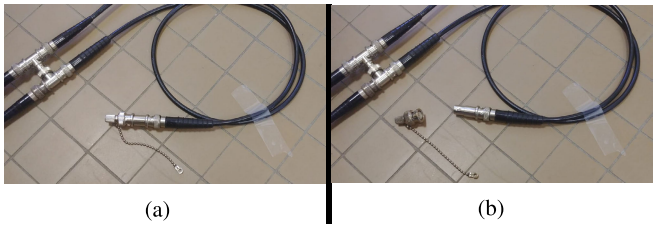

Fig. 14. Removing the 50-Ω resistor at the termination of the cable. (a) Healthy termination. (b) Faulty termination.

Here, we interpret and justify the obtained results. At first, the idea behind starting from a simple configuration is the theoretical ease of expecting the solution beforehand by a simple analysis of the signal propagation in Ω_H and Ω_F. Obviously, in Ω_H, no multiple reflections occur in the cables due to their matched loads at all the terminations. As a result, the only signal reaching the oscilloscope is that propagating directly through the linking paths AWG-CH_1 and AWG-CH_2. In Ω_F, the recorded signals, after injecting $\boldsymbol{\alpha}$, can be analyzed as follows: the first two peaks correspond to the signal traveling directly through the linking paths AWG-CH_1 and AWG-CH_2. The third and the fourth peaks appear due to the signal reaching the faulty termination and then reflecting back toward CH_1 and CH_2. Theoretically, the source $\mathbf{x}$ to be computed by the LCCF is the signal $\boldsymbol{\alpha}$ with additional peaks opposite to the sign of the distortions. These expectations perfectly match the source $\mathbf{x}$ computed by the LCCF method. In fact, the additional peaks of $\mathbf{x}$ and the distortions intersect at the appropriate instants of time to cancel one another according to the superposition theorem. The LCCF also cancels the peaks resulting from the multiple reflections of its source. Recording over a long time interval assures that the correction is achieved over the desired time interval without signal amplification.

B. Hard Fault

Hard faults, like soft faults, cause time and money losses if they are inaccessible or not immediately accessible. Add to that, they may jeopardize the functioning of the overall system, resulting in data breaks and fires. They are, therefore, regarded as critical situations and necessitate taking action in the shortest time, such as the EC. Herein, we conduct an experimental test to show that the EC process remains applicable in the presence of a hard fault. A hard fault may be an open or a short circuit and may be located at any network position as long as the receiver is still receiving signals. More precisely, if we assume that a hard fault appeared on any direct path between the generator and any of the receiver points, the EC is not applicable at this receiver point, in such a particular case. Alternatively, other wire diagnosis techniques (e.g., reflectometry) are required to locate the fault(s). Such

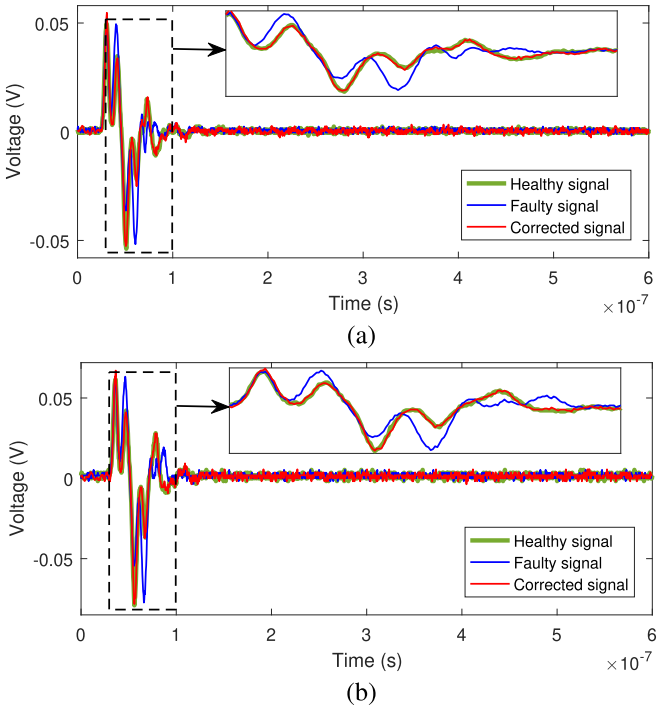

Fig. 15. Experimental EC of the faulty network presenting a single hard fault. (a) Healthy, faulty, and corrected voltage signals at CH_1. (b) Healthy, faulty, and corrected voltage signals at CH_2.

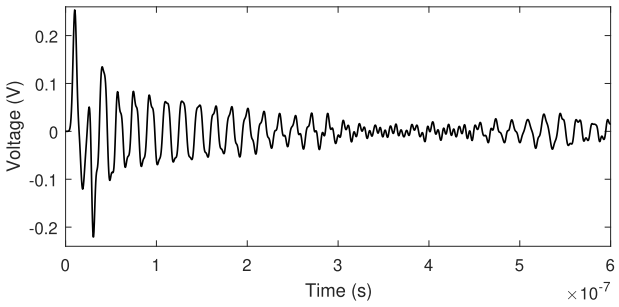

Fig. 16. Source $\mathbf{x}$ computed to correct the outputs in the presence of a single hard fault.

techniques may necessitate prior knowledge of the network's configuration.

1) Network Configuration: To show that the EC process is applicable to more complex configurations, the network Ω_H of Fig. 13 composed of nine standard 50-Ω coaxial cables and three junctions is considered. The cables' length, Z_C, and Z_L are displayed in Table III.

2) Electrical Correction: Let the hard fault be an open circuit and modeled by removing the 50-Ω resistor at the termination of line 2 (see Fig. 14). The fault is represented by the black X-mark in Fig. 13(b). The separate injection of $\boldsymbol{\alpha}$ in Ω_H and Ω_F indicates a high distortion of the outputs at CH_1 and CH_2, as shown in Fig. 15. Based on these outputs, the LCCF system is solved and then switched to the canonical basis to compute the source $\mathbf{x}$ displayed in Fig. 16. The source $\mathbf{x}$ is more complex in this case due to more reflections and re-reflections to be canceled in a complex network configuration. Injecting $\mathbf{x}$ in Ω_F corrects the outputs at CH_1 and CH_2, as seen in Fig. 15.

TABLE III
CHARACTERISTICS OF THE NETWORK OF FIG. 13

Line Nb.	Length (in m)	Z_C (in Ω)	Z_L (in Ω)
1	1.2	50	-
2	0.8	50	50
3	1.2	50	-
4	1	50	∞
5	2	50	-
6	2	50	50
7	3	50	50
8	1	50	50
9	1.2	50	∞

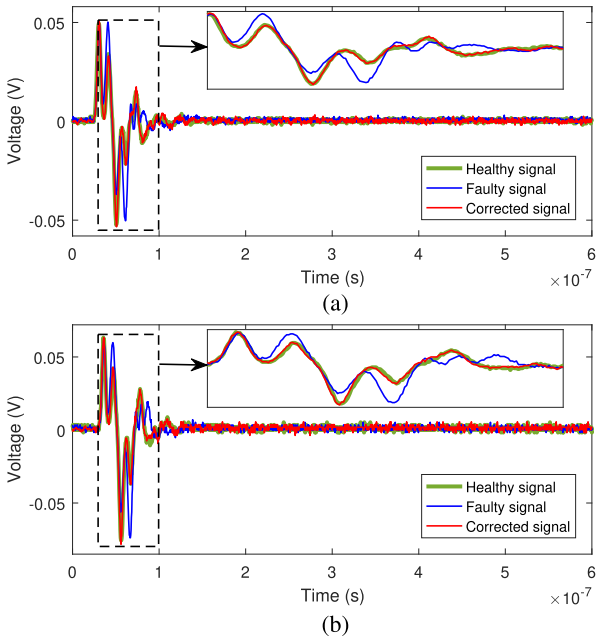

Fig. 17. Experimental EC of the faulty network presenting multiple faults (soft and hard). (a) Healthy, faulty, and corrected voltage signals at CH_1. (b) Healthy, faulty, and corrected voltage signals at CH_2.

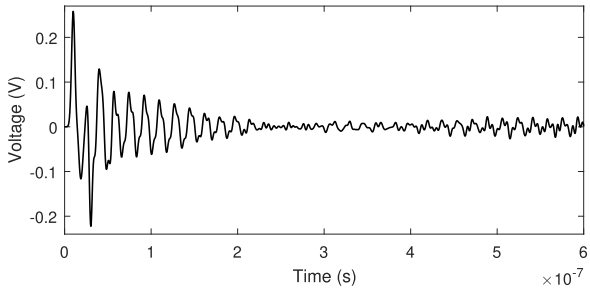

Fig. 18. Source $\mathbf{x}$ computed to correct the outputs in the presence of multiple faults (soft and hard).

C. Multiple Faults

1) Network Configuration: See Section VI-B1.

2) Electrical Correction: To test the case of multiple faults, we keep the hard fault of Section VI-B at the end of line 2 and introduce an additional soft fault located at the termination of line 8 [see the gray X-mark in Fig. 13(b)]. This latter is modeled by modifying Z_L from 50 to 82.5 Ω. The results in

Fig. 17 show that the EC process efficiently cancels the effects of the multiple faults after injecting the source **x** (see Fig. 18) computed by the LCCF method.

Apparently, Figs. 15 and 17 may look the same although the former corresponds to bringing an EC to the faulty network presenting a single hard fault, while the latter corresponds to bringing an EC to the faulty network presenting multiple faults. This resemblance indicates that either the effect of the soft fault is quite low compared to that of the hard fault or the distortions caused by the soft fault are completely attenuated before reaching the oscilloscope. Nevertheless, the computed sources in both cases by the LCCF method (Figs. 16 and 18) are slightly different. Such a difference demonstrates the ability of the LCCF method to compensate for the effect of the soft fault even if it may not be observed at the oscilloscope level. It should be emphasized that it is still possible to introduce faults of any nature at any position on the cables as long as the oscilloscope still receives signals.

VII. Conclusion

With a view to considering experimental tests and practical applications, the LCCF method in this article was modified to comply with some limitations encountered during experiments. More precisely and due to the impossible record of a Dirac signal between the input–output points in experiments, an efficient solution was suggested to record the response of any nonnull signal between the input–output points and not necessarily the impulse response. After describing the experimental setup, the LCCF in its version adapted to experiments was tested to identify the profile of voltage/current time-domain sources to impose a desired target voltage/current at some points of the network over a predefined time interval. Then, in the context of faulty TL networks, the LCCF was also tested to bring an EC to some networks' terminations regardless of the number, nature, and positions of the potential electrical faults. For both experimental validations, simple, ramified, and complex networks with different characteristics were considered to prove the generality of the LCCF method.

Forthcoming works may handle features that have not been addressed up to the moment, such as developing the LCCF method to identify sources whose frequencies lie in a predefined bandwidth. It could also be interesting to test the LCCF on other cable types, such as twisted pair cables or complex cable bundles.

Acknowledgment

The authors would like to thank Sébastien Girard for his technical help in the experimental validations of the LCCF method.

References

[1] S. Zhenfei, S. Donglin, D. Fei, F. Duval, and A. Louis, "A novel electromagnetic radiated emission source identification methodology," in *Proc. Asia–Pacific Int. Symp. Electromagn. Compat.*, Apr. 2010, pp. 645–648.

[2] H. Göksu, D. C. Wunsch, X. Dong, A. Kökce, and D. G. Beetner, "Detection and identification of vehicles based on their spark-free unintended electromagnetic emissions," *IEEE Trans. Electromagn. Compat.*, vol. 60, no. 5, pp. 1594–1597, Oct. 2018.

[3] M. D'Amore, A. Morriello, and M. S. Sarto, "A neural network approach for identification of EM field sources: Analysis of PCB configurations," in *Proc. IEEE EMC Symp. Int. Symp. Electromagn. Compat. Symp. Rec.*, vol. 2, Aug. 1998, pp. 664–669.

[4] J. L. A. Quijano and G. Vecchi, "Field and source equivalence in source reconstruction on 3D surfaces," *Prog. Electromagn. Res.*, vol. 103, pp. 67–100, 2010.

[5] B. Liu, L. Beghou, L. Pichon, and F. Costa, "Adaptive genetic algorithm based source identification with near-field scanning method," *Prog. Electromagn. Res. B*, vol. 9, pp. 215–230, 2008.

[6] F. Benyoubi, L. Pichon, M. Bensetti, Y. Le Bihan, and M. Feliachi, "An efficient method for modeling the magnetic field emissions of power electronic equipment from magnetic near field measurements," *IEEE Trans. Electromagn. Compat.*, vol. 59, no. 2, pp. 609–617, Apr. 2017.

[7] R. Albanese and P. B. Monk, "The inverse source problem for Maxwell's equations," *Inverse Problems*, vol. 22, no. 3, pp. 1023–1035, Jun. 2006.

[8] T. K. Sarkar and A. Taaghol, "Near-field to near/far-field transformation for arbitrary near-field geometry utilizing an equivalent electric current and MoM," *IEEE Trans. Antennas Propag.*, vol. 47, no. 3, pp. 566–573, Mar. 1999.

[9] F. Las-Heras and T. K. Sarkar, "A direct optimization approach for source reconstruction and NF-FF transformation using amplitude-only data," *IEEE Trans. Antennas Propag.*, vol. 50, no. 4, pp. 500–510, Apr. 2002.

[10] M. Spirlet, C. Geuzaine, and V. Beauvois, "Optimal control theory applied to unintended source control and field shaping for time-harmonic electromagnetic waves," *IEEE Trans. Electromagn. Compat.*, vol. 62, no. 1, pp. 65–73, Feb. 2020.

[11] M. Spirlet, "Correction of electromagnetic measurements and active shaping of electromagnetic fields in complex and reverberating environments," Ph.D. dissertation, Montefiore Inst. Elect. Eng. Comput. Sci., Univ. Liége, Belgium, Brussels, Belgium, 2017, pp. 59–74.

[12] M. Fink, "Time reversal of ultrasonic fields: Part I. Basic principles," *IEEE Trans. Ultrason., Ferroelectr., Freq. Control*, vol. 39, no. 5, pp. 555–556, Sep. 1992.

[13] P. Bonnet, S. Lalléchére, and F. Paladian, "From electromagnetic time-reversal theoretical accuracy to practical robustness for EMC applications," in *Electromagnetic Time Reversal: Application to Electromagnetic Compatibility and Power Systems*, F. Rachidi, M. Rubinstein, and M. Paolone, Eds. Hoboken, NJ, USA: Wiley, pp. 91–144, 2017.

[14] M. Kafal and A. Cozza, "Multifrequency TR-MUSIC processing to locate soft faults in cables subject to noise," *IEEE Trans. Instrum. Meas.*, vol. 69, no. 2, pp. 411–418, Feb. 2020.

[15] S. Mariano, A. Massa, M. Pastorino, and A. Randazzo, "Experimental validation of a time reversal technique for ultra-wideband antenna localization," *IEEE Trans. Antennas Propag.*, vol. 67, no. 8, pp. 5347–5356, 2019.

[16] X. Chen, Y. Zhang, J. Ma, and H. Chen, "Experimental study of a time-reversal-based method for electromagnetic interference source localization," *IEEE Access*, vol. 7, pp. 108658–108666, 2019.

[17] S. Lalléchère, P. Bonnet, B. Jannet, and L. Berry, "Electromagnetic time reversal robustness for EMC applications," in *Proc. 1st URSI Atlantic Radio Sci. Conf. (URSI AT-RASC)*, May 2015, p. 1.

[18] W. M. G. Dyab, T. K. Sarkar, A. García-Lampérez, M. Salazar-Palma, and M. A. Lagunas, "A critical look at the principles of electromagnetic time reversal and its consequences," *IEEE Antennas Propag. Mag.*, vol. 55, no. 5, pp. 28–62, Oct. 2013.

[19] A. Cozza, "Statistics of the performance of time reversal in a lossy reverberating medium," *Phys. Rev. E, Stat. Phys. Plasmas Fluids Relat. Interdiscip. Top.*, vol. 80, no. 5, Nov. 2009, Art. no. 056614.

[20] Z. Wang, R. Razzaghi, M. Paolone, and F. Rachidi, "Time reversal applied to fault location in power networks: Pilot test results and analyses," *Int. J. Electr. Power Energy Syst.*, vol. 114, Jan. 2020, Art. no. 105382.

[21] M. Kafal, R. Razzaghi, A. Cozza, F. Auzanneau, and W. B. Hassen, "A review on the application of the time reversal theory to wire network and power system diagnosis," in *Proc. IEEE Int. Instrum. Meas. Technol. Conf. (I2MTC)*, May 2019, pp. 1–6.

[22] M. Kafal, A. Cozza, and L. Pichon, "Locating multiple soft faults in wire networks using an alternative DORT implementation," *IEEE Trans. Instrum. Meas.*, vol. 65, no. 2, pp. 399–406, Feb. 2016.

[23] L. El Sahmarany, L. Berry, N. Ravot, F. Auzanneau, and P. Bonnet, "Time reversal for soft faults diagnosis in wire networks," *Prog. Electromagn. Res. M*, vol. 31, pp. 45–58, 2013.

[24] F. Auzanneau, "Wire troubleshooting and diagnosis: Review and perspectives," *Prog. Electromagn. Res. B*, vol. 49, pp. 253–279, 2013.
[25] C. Furse, Y. C. Chung, C. Lo, and P. Pendayala, "A critical comparison of reflectometry methods for location of wiring faults," *Smart Struct. Syst.*, vol. 2, no. 1, pp. 25–46, Jan. 2006.
[26] J. Benoit, C. Chauvière, and P. Bonnet, "Source identification in time domain electromagnetics," *J. Comput. Phys.*, vol. 231, no. 8, pp. 3446–3456, Apr. 2012.
[27] J. Benoit, C. Chauvière, and P. Bonnet, "Time-dependent current source identification for numerical simulations of Maxwell's equations," *J. Comput. Phys.*, vol. 289, pp. 116–128, May 2015.
[28] V. Mazières et al., "Transient electric field shaping with the linear combination of configuration field method for enhanced spatial control of microwave plasmas," *IEEE Access*, vol. 8, pp. 177084–177091, 2020.
[29] A. Al Ibrahim, C. Chauvière, and P. Bonnet, "Active electromagnetic interference control in time domain: Application to software correction of defective lossy transmission-line networks," *IEEE Trans. Electromagn. Compat.*, vol. 62, no. 2, pp. 355–363, Apr. 2020.
[30] L. Abboud, A. Cozza, and L. Pichon, "A matched-pulse approach for soft-fault detection in complex wire networks," *IEEE Trans. Instrum. Meas.*, vol. 61, no. 6, pp. 1719–1732, Jun. 2012.
[31] A. Al Ibrahim, "Linear and nonlinear numerical methods for real-world inverse problems of time-domain electromagnetic active shaping—From theory to experiment," Ph.D. dissertation, Inst. Pascal, Univ. Clermont Auvergne, France, Clermont-Ferrand France, 2021.
[32] A. Al Ibrahim, C. Chauvière, and P. Bonnet, "Time-domain software correction of nonlinear faulty lossy transmission line networks," *IEEE Trans. Electromagn. Compat.*, vol. 62, no. 4, pp. 1304–1311, Aug. 2020.
[33] A. A. Ibrahim, C. Chauvière, and P. Bonnet, "Software correction of defective lossy transmission line networks," in *Proc. Photon. Electromagn. Res. Symp. Spring (PIERS-Spring)*, Jun. 2019, pp. 3102–3108.
[34] A. N. Tychonoff, "Solution incorrectly formulated problems and the regularization method," *Sov. Math.*, vol. 4, pp. 1035–1038, 1963.
[35] A. Al Ibrahim, C. Chauvière, and P. Bonnet, "Active shaping of voltage/current in transmission lines–EMC/Si applications," in *Proc. Int. Conf. Electromagn. Adv. Appl. (ICEAA)*, Sep. 2019, pp. 26–30.

Ali Al Ibrahim received the M.Sc. degree in applied mathematics from the University of Strasbourg, Strasbourg, France, in 2017, and the Ph.D. degree in electronics and systems from Institut Pascal, University of Clermont Auvergne, Clermont-Ferrand, France, in 2021.

He was a Post-Doctoral Researcher at France Energies Marines, Plouzané, France, from 2021 to 2023. Currently, he is working for renowned energy production companies where he addresses a diverse range of inquiries related to wire diagnosis, power cable systems, electromagnetic compatibility, and lightning protection.

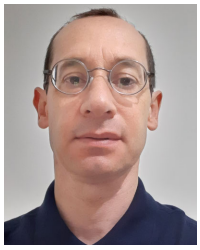

Cédric Chauvière received the Ph.D. degree in mechanical engineering from the École Polytechnique Fédérale de Lausanne, Lausanne, Switzerland, in 2001.

He conducted Post-Doctoral Research at the Department of Applied Mathematics, Brown University, Providence, RI, USA, from 2002 to 2003. He is currently the Maître de Conférence of mathematics with the University of Clermont Auvergne, Clermont-Ferrand, France. His current research interests include artificial intelligence, uncertainty quantification, electromagnetic source identification, and numerical methods for stochastic problems.

Pierre Bonnet received the Diploma Engineer degree in physics from Polytech Clermont-Ferrand, Clermont-Ferrand, France, in 1994, and the M.Sc. and Ph.D. degrees in electromagnetism from Blaise Pascal University, Aubiére, France, in 1994 and 1998, respectively.

From 1999 to 2008, he was an Assistant Professor with the Department of Physics and the Institut Pascal, Blaise Pascal University. He is currently a Full Professor with Clermont Auvergne University, Clermont-Ferrand, where he is also the Head of the Electromagnetic Compatibility Group. His current research interests include numerical electromagnetic with an emphasis on electromagnetic compatibility/electromagnetic interference problems, electromagnetic shielding, reverberating electromagnetic environment, time reversal, source identification, and stochastic modeling.